LATEST RESULTS FROM THE TELESCOPE ARRAY

P. Tinyakov,
for the Telescope Array collaboration
Service de Physique Théorique CP225, Université Libre de Bruxelles, Blvd du Triomphe, 1050 Bruxelles

The Telescope Array (TA) is a hybrid detector of ultra-high energy cosmic rays situated in Utah, USA. It is aimed at studying cosmic rays with energies up to, and exceeding 10^{20} eV by detecting giant airshowers they produce in the atmosphere. The detector is taking data since March 2008. We will present the latest results of the spectrum, composition and anisotropy studies based on the 7 years of the TA data.

1 Introduction

Cosmic ray (CR) energy spectrum extends from ∼GeV energies to as high as 10^{11} GeV and beyond. At highest energies the CR flux becomes so tiny that thousands of square kilometers of effective area is needed to measure it. In current detectors, Earth atmosphere is used as a target. The ultra-high energy incident particles hit the atmosphere and produce giant air showers. These air showers are detected in several ways: by the array of particle detectors placed on the ground, by the telescopes registering the fluorescent and/or the Cherenkov light emitted by the shower, or by the array of radio antennas detecting the radio signal from the shower.

The aim of the Telescope Array (TA) experiment is to detect and study ultra-high energy cosmic rays (UHECRs) by observing the giant air showers they produce in the atmosphere, with the ultimate goal of discovering the nature and origin of these highest energy particles. It combines several of the detection techniques: the surface array of particle detectors, and the UV telescopes capable of detecting the fluorescent and Cherenkov light. Different detection methods complement each other: the surface array has the duty cycle close to $\sim 95\%$ and thus the largest statistics; the fluorescence telescopes provide one with a calorimetric shower energy measurement, allow one to reconstruct the shower longitudinal profile and also have lower energy threshold; the observation of Cherenkov light make it possible to extend the energy threshold even lower.

The data collected by the TA detectors allow one to reconstruct the original directions of the primary particles and their energies, as well as to determine, on a statistical basis, the UHECR mass composition. Below we will review the results of TA concerning the energy spectrum, mass composition and anisotropies of UHECR.

2 The Telescope Array Detector

The Telescope Array (TA) is a hybrid detector of ultra-high energy cosmic rays (UHECR) located in the Northern hemisphere in Utah, USA ($39^\circ 17' 48''$ N, $112^\circ 54' 31''$ W) at the elevation of $\sim$ 1400m above the sea level. It currently consists of the surface detector (SD) composed of

507 scintillator detectors covering the area of approximately 700 km^2 with the spacing of 1.2km (for details see [1]). Each detector is completely autonomous, consisting of a 3 m^2 2-layer plastic scintillator monitored by 2 PMTs, powered by a solar panel and connected by radio. The TA detector is fully operational starting from March 2008.

The atmosphere over the surface array is viewed by 38 fluorescence telescopes arranged in 3 stations [2], which constitute the fluorescence detector (FD) of TA. The stations are referred to as Middle Drum (MD, the refurbished HiRes telescope), the Black Rock Mesa (BR) and the Long Ridge (LR). These stations view 112° (108°) in azimuth and $3° - 31°$ ($3° - 33°$) in the zenith angle in case of MD (BR/LR). Each individual telescope consists of a mirror (5.2m^2 for MD, 6.8m^2 for BR/LR) focusing the collected light on a square array of 256 PMTs of about 1 m^2. As the shower develops in the field of view of the telescope, its image moves across the array of PMTs. The light intensity and time information is registered.

In 2014 the low-energy extension of TA (TALE) has been constructed at the Middle Drum site that consists of a denser ground array (spacing 400 m) overlooked by a dedicated station comprising 10 fluorescence telescopes with higher elevation ($31° - 59°$) of the viewing angle optimized for a lower energy threshold.

3 The Data

The surface detector samples the giant air shower at the ground level at the positions of individual SD detectors. Each triggered detector records the deposited energy and the timing information. These data are then used to reconstruct the shower geometry giving the direction of the incident particle, and the lateral shower profile (the density of charged particles as a function of the distance from the core) which characterizes the incident particle energy. The density of charged particles at 800 m from the shower core, S800, is used as the energy estimator. For a given shower with a given zenith angle, the energy is calculated from S800 by means of a look-up table obtained in a complete Monte-Carlo simulation of the detector. The resulting energy is divided by the calibration factor 1.27 (see below) to give the true energy of the shower. The larger the shower energy, the larger the number of detectors that are triggered and the higher the precision of reconstructed parameters. Above the energy of 10^{19} eV the efficiency of the TA SD is close to 100%; it decreases gradually at lower energies. The energy spectrum can be reconstructed from the SD data at energies above $10^{18.2}$ eV. The total exposure of TA SD accumulated in the first 7 years of operation is 6300 km^2 sr yr

The FD telescopes register the fluorescent light emitted by the shower. The total amount of light is proportional to the number of charged particles and thus to the energy of the shower. This gives a nearly calorimetric energy measurement. If the fluorescent yield per particle is know, integrating the emitted light along the shower profile measured by the FD with proper account of the distance and atmospheric effects, allows one to reconstruct the energy of the incident particle. The details of the FD energy estimation can be found in [3].

The hybrid design of the TA detector makes it possible to calibrate the SD energy estimation to the (*a priori* more accurate) FD one. This method is currently adopted by both TA and Pierre Auger experiments. The comparison of the FD and SD energies for hybrid events (i.e., events that have been detected by the SD and by at least one of the FD stations) shows the linear dependence between the two energy scales, with the SD energy being a factor 1.27 higher. The SD energies reported below are scaled down by this factor, unless stated otherwise.

4 The energy spectrum

The energy spectrum of UHECR is measured by TA in several complementary ways. The results of these measurements are presented in Fig. 1 which shows the SD spectrum (black), the FD spectrum (blue) and TALE FD (red filled) as well as TALE Cherenkov (red empty) spectra.

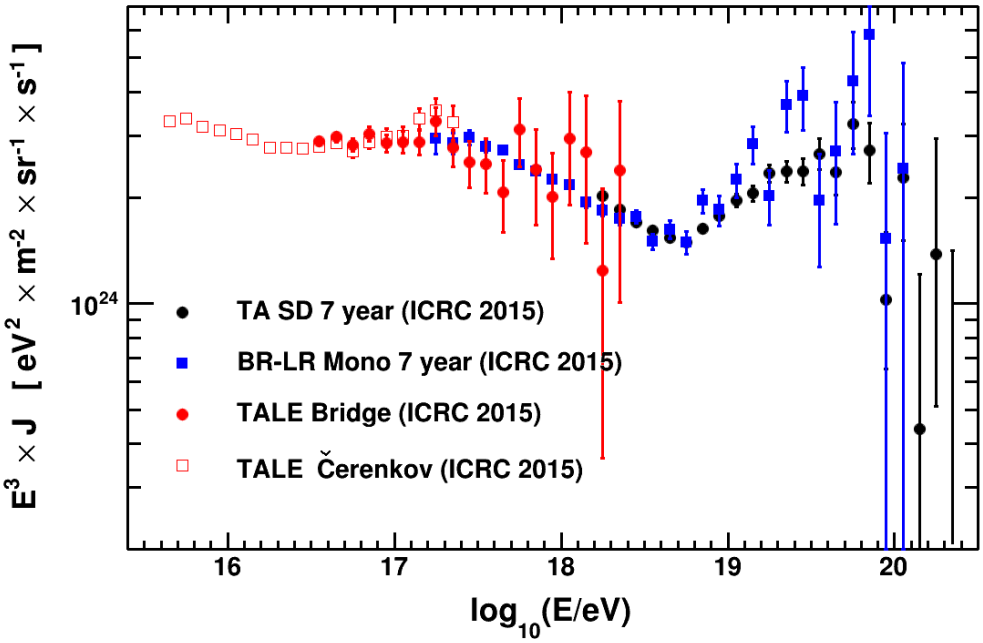

Figure 1 – The TA energy spectra obtained from the SD, FD mono, TALE and TALE Cherenkov data as indicated on the plot.

The SD spectrum starts above $10^{18.2}$ eV and extends to the highest energies. The FD spectrum goes down in energy by an order of magnitude. The TALE FD and Cherenkov extend another two orders towards low energies. One can see from the plot that these spectra overlap with each other, and are consistent in the overlap regions. Thus, one can combine them into a single spectrum that covers the energy range extending over 4.5 orders of magnitude.

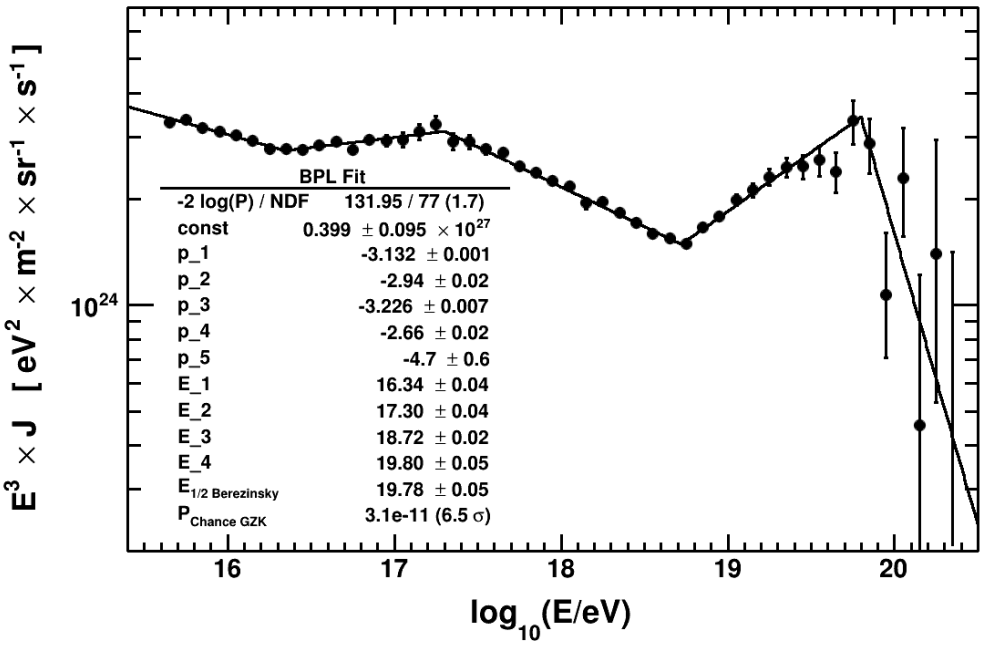

Figure 2 – The combined TA energy spectrum (black points) fitted to a broken power law (black line). The results of the fit are summarized on the plot.

The combined TA spectrum obtained in this way is presented in Fig. 2 by points with error bars. It can be fitted rather well by a broken power law. The results of the fit are also shown in Fig. 2 by lines. Several features are clearly visible: the hardening at $10^{16.34\pm0.04}$ eV, the knee at $10^{17.3\pm0.04}$ eV, the ankle at $10^{18.72\pm0.02}$ eV and the break at $10^{19.80\pm0.05}$ eV.

The significance of the highest-energy break is 6.5σ. Its position is compatible with the GZK cutoff for protons. Indeed, the GZK cutoff may be characterized by $E_{1/2}$, the energy at which the integral spectrum falls to one half of its expected value in the absence of the cutoff. This value is predicted to be $10^{19.72}$ eV [4]; the TA measurement gives $\log_{10} E_{1/2} = 19.78 \pm 0.05$ in good agreement with the pure proton model.

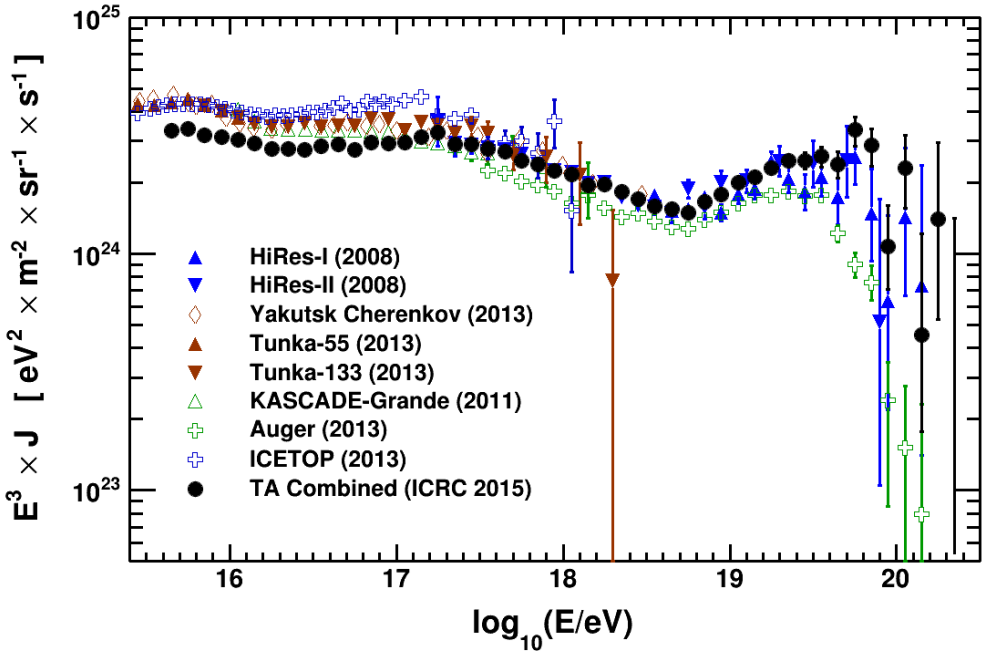

Figure 3 – The comparison of the TA energy spectrum with the results of other experiments as indicated on the plot.

The comparison of the TA energy spectrum with the results of other experiments is shown in Fig. 3. As one can see, all the features visible in the TA spectrum are also present in other experiments, possibly shifted in energy due to the systematic errors in the energy determination. In particular, the Auger spectrum agrees well in shape with the TA one, except in the GZK region. Below the GZK, the two spectra may be made compatible by a relative energy rescaling by $\sim 15\%$. If such a shift is performed, the spectra still disagree at highest energies — at and above the cutoff. One of the possible reasons for this disagreement could be the difference between Northern and Southern hemispheres. Another reason could be energy dependence of the systematic difference in the Auger and TA energy scales.

5 Mass composition

The main observable sensitive to the nature of primary particle is the shower depth $X_{\max}$, the atmospheric depth of the maximum of the shower. This quantity can only be directly measured by the fluorescent detector, so the FD data have to be used in the composition analysis. For a given shower, $X_{\max}$ depends on the depth of the first interaction, and on the development of the shower. Showers initiated by protons have larger $X_{\max}$ on average than those initiated by nuclei. The difference in mean $X_{\max}$ between proton and iron is of order ~ 80 g/cm^2, with the exact value depending on the hadronic interaction model.

Even for the same primary species, $X_{\rm max}$ fluctuates strongly from shower to shower, making it impossible to determine the composition on event-by-event basis, at least from $X_{\rm max}$ alone. These fluctuations are larger for protons and smaller for heavier nuclei.

The measurement of the UHECR composition from the distribution of $X_{\rm max}$ is not straightforward because the FD event sets are generically biased with respect to this variable: accurate reconstruction requires that the maximum of the shower is within the field of view of the FD detector. The strategy adopted in TA is to simulate the observed event set taking all the selection biases into account, and compare the simulated distribution of the $X_{\rm max}$ for different primary particles with the observed one. This has to be kept in mind when comparing the composition measurements by TA and Auger which adopts a different measurement strategy.

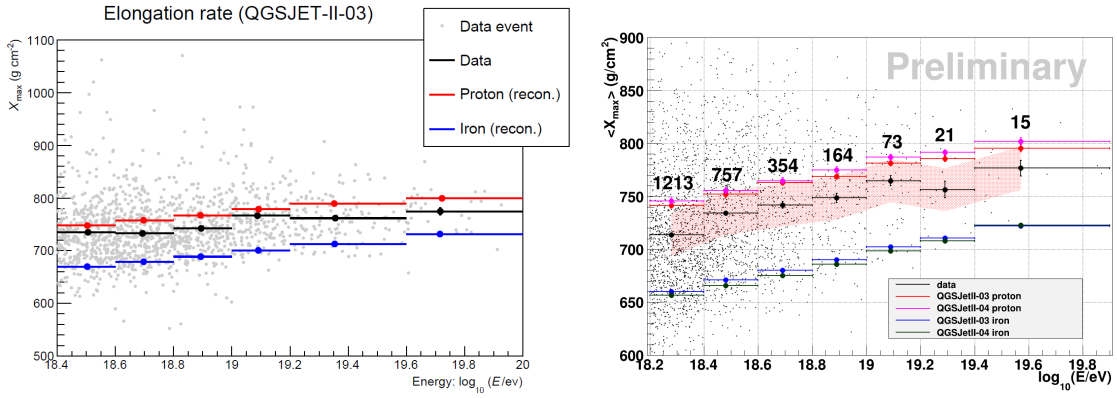

Figure 4 – *Left panel:* The elongation rate as measured from the TA stereo data, all stations. Black dots: data; red (blue) dots: simulations for proton (iron); gray dots: actual events. *Right panel:* The elongation rate as measured from the TA hybrid data, all stations. Black: data; other colors: simulations for proton (iron) with different interaction models as indicated in the legend; small black dots: actual events. The pink band represents the estimated systematic uncertainty.

Fig. 4, left panel, shows the $X_{\rm max}$ measurement using the stereo TA data (1347 events, all 3 FD stations). The black dots with error bars represent the data, the red (blue) dots correspond to the MC simulation assuming protons (iron) and QGSJET-II-03 hadronic interaction model. Gray dots represent actual events. The pure proton composition is favored over pure iron one at all energies.

On Fig. 4, right panel, we show the $X_{\rm max}$ measurement with the hybrid events (all FD stations). This is the largest-statistics measurement involving 2597 events with energies above $10^{18.2}$ eV. The black dots with error bars represent the data; other colors represent proton/iron MC simulations with two different hadronic interaction models as indicated on the plot. Small black dots represent the actual events. The pink band corresponds to the estimated systematic uncertainty. As one can see from this plot, a light composition is favored by the TA measurement.

As has been already mentioned, the comparison of the TA and Auger composition measurements is not straightforward because of a different treatment of the observational bias. To perform such a comparison, a mixture of nuclei has been prepared such that it fits the Auger $\langle X_{\rm max}\rangle$ and $\Delta X_{\rm max}$ measurements. This mixture then has been passed through the TA reconstruction chain and $\langle X_{\rm max}\rangle$ has been extracted. The result of this numerical experiment is compared to the actual TA measurement in Fig. 5. The reconstructed Auger mix is shown in red, the actual TA measurement in blue. Also shown is the MC expectation for proton and iron. One can see a very good agreement between the actual measurement and the simulated result assuming the Auger mix. Thus, the TA measurement cannot exclude a light composition similar to the Auger mix.

To conclude this section, consider the limits on the UHE photon flux. Although the dominant fraction of photons in the UHECR flux is excluded, it is important to set quantitative limits on this fraction because sizeable fractions of photons are predicted in some models of UHECR. A

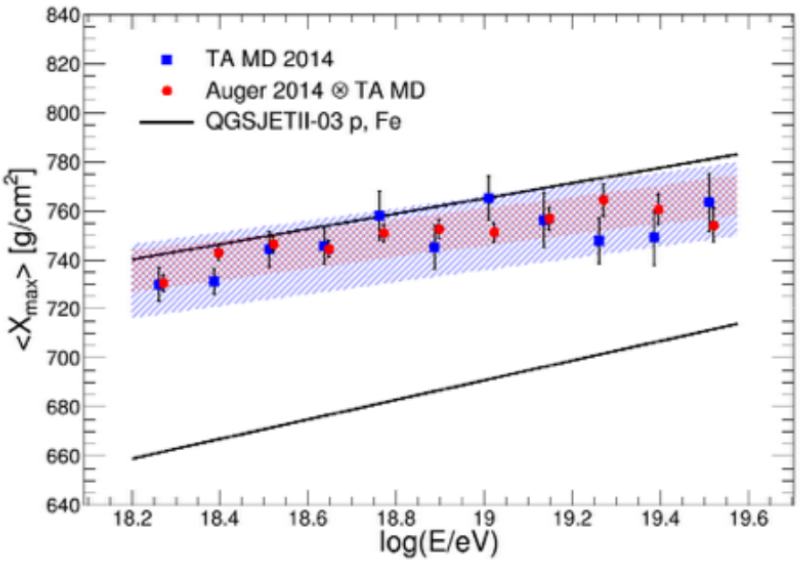

Figure 5 – The comparison between the TA $\langle X_{\rm max}\rangle$ measurement (blue squares) and the simulation assuming the mixed composition that fits best the Auger data (red circles). Black lines show expectation in case of pure proton/iron composition.

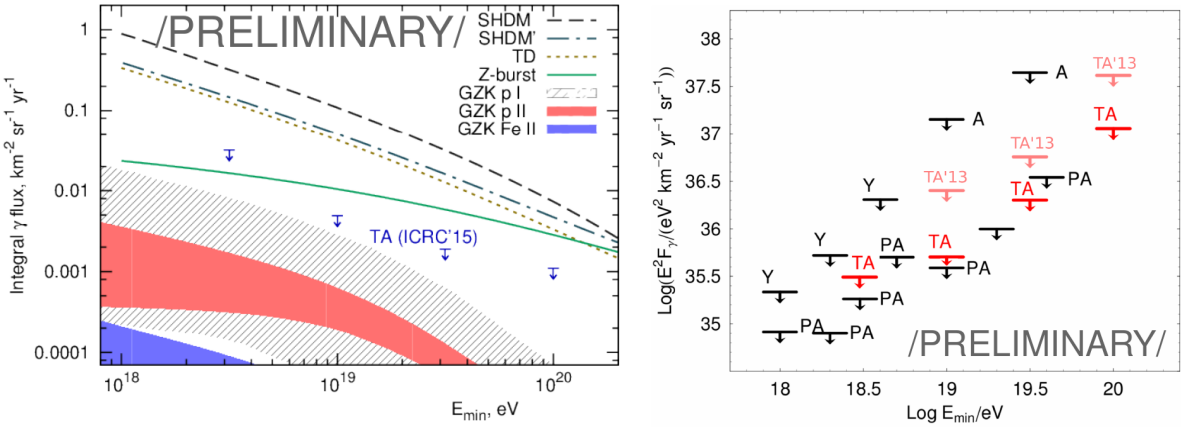

Figure 6 – *Left panel:* TA limit on the photon flux in comparison with expectations in some UHECR models. *Right panel:* comparison of TA limits with the results of other experiments: Auger (labeled PA), AGASA (labeled A), Yakutsk (labeled Y), previous TA result (labeled TA13).

dedicated analysis has been performed in TA to set such limits. Several composition-sensitive observables have been combined into a single estimator by the Boosted Decision Tree (BDT) technique. The algorithm was trained on the MC simulations and then applied to the data. The results are presented in Fig. 6. Left panel show the TA limits on the photon flux at different energies compared to expectations in several UHECR models as indicated on the plot. The right panel compares TA limits with the results of other experiments.

6 Anisotropy Searches

6.1 Anisotropy Data

Most UHECR anisotropy searches are limited by statistics. At the same time the reconstruction of arrival directions is very robust and free from systematic errors. One can relax some of the cuts and substantially gain in the number of reconstructed events without loosing much in their quality. Following this idea, a special data set is used in TA for anisotropy studies. Most of

the increase in statistics comes form relaxing the zenith angle cut to $z < 55°$ and loosening the border cut. The full description of this set can be found in Ref. [5].

By comparing the thrown and reconstructed arrival directions of the simulated data sets, the angular resolution of TA events from the anisotropy set was found to be approximately 1.5°. Events with zenith angles between 45° and 55° have even better angular resolution. The energy resolution of the events at $E > 10$ EeV is close to 20% [6].

In anisotropy studies it is important to know well the exposure function. The exposure of the TA SD detector is calculated by the Monte-Carlo technique with the full simulation of the detector. It follows from these simulations that above 10 EeV the efficiency of the TA SD is 100%, while the exposure is indistinguishable from the geometrical one at present statistics.

To avoid statistical penalties for scanning over energy threshold, TA uses three *a priori* defined thresholds: 10 EeV, 40 EeV and 57 EeV wherever appropriate. The 7-yr anisotropy set contains 2996 events above 10 EeV, 210 events above 40 EeV and 83 events above 57 EeV.

6.2 Global Distributions

We first present the global distribution of the TA events. To search for possible large-scale deviations from isotropy we perform a simple Kolmogorov-Smirnov test comparing the distributions of events in latitude and longitude with that expected for the isotropic event distribution modulated with the exposure function. This test was performed in two coordinate systems: equatorial and supergalactic.

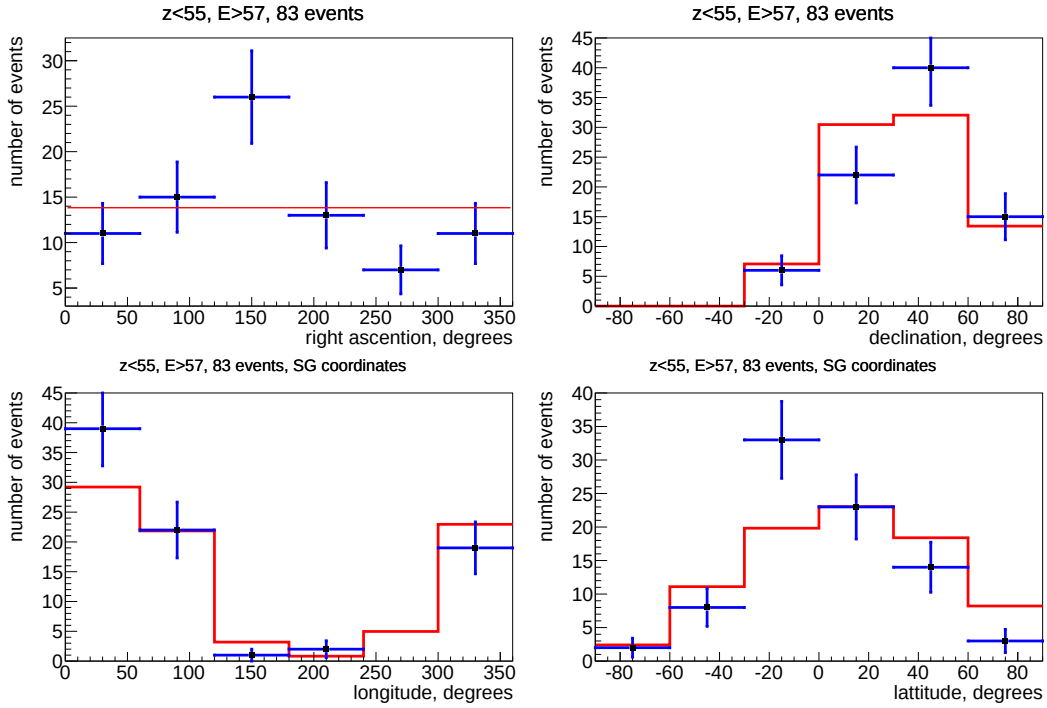

Figure 7 – The distributions of 83 events with $E > 57$ EeV (blue points with error bars) in longitude and latitude in equatorial and supergalactic coordinate systems, as marked on the plots. Red histogram shows the expectation assuming isotropic distribution.

The two low-energy subsets with energy thresholds of 10 EeV and 40 EeV show no deviations from isotropy in any of the 4 tests. The smallest p-value found was 0.12. The highest-energy subset with $E > 57$ EeV shows a mild deviation from isotropy: in equatorial coordinates the p-values for the compatibility with isotropy are 0.07 and 0.04 for longitude and latitude, respectively, while in supergalactic coordinates the corresponding numbers are 0.01 and 0.03. The histograms of events are presented in Fig. 7.

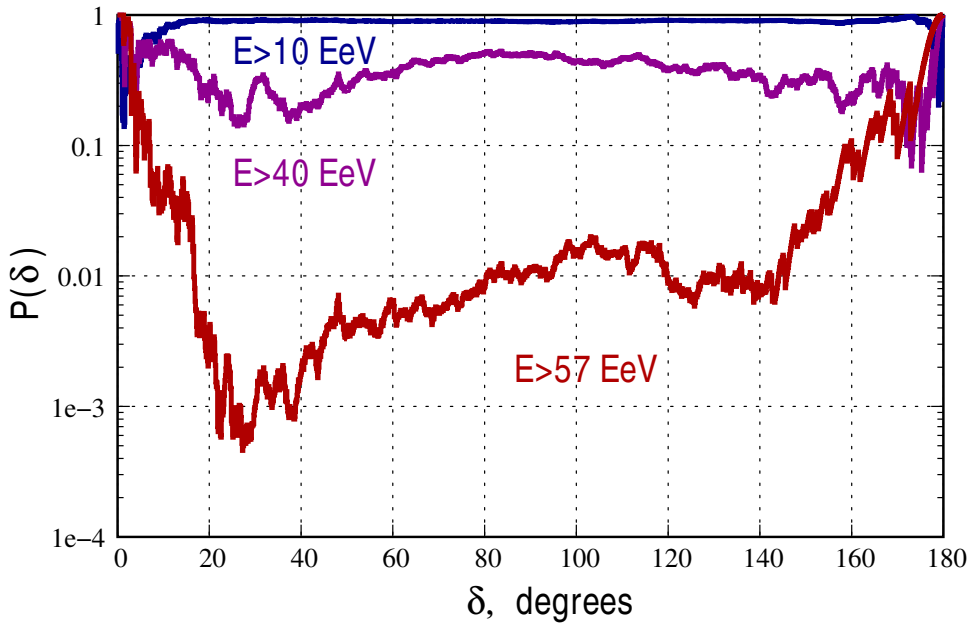

Figure 8 – The p-value $P(\delta)$ that characterizes the significance of the excess in the number of pairs of TA events separated by angles less than δ, for three subsets with different energy thresholds as marked on the plot.

Another way the anisotropy may manifest itself is in the angular correlation function. The latter can be calculated as follows. In the data one counts the number of pairs of events separated by angular distances within the i-th angular bin and obtains the data counts $N_i^{\rm data}$. One then generates a large number of Monte-Carlo event sets, each having the same number of events as the data. The simulated events follow the isotropic distribution modulated with the exposure. In each set the number of pairs of events is calculated as in the data; the average over the MC sets is then taken giving $\langle N_i^{\rm MC}\rangle$ (not necessarily integer). The angular correlation function at an angular scale corresponding to the i-th angular bin is proportional to $N_i^{\rm data} - \langle N_i^{\rm MC}\rangle$. In practice, because of small statistics, one often works with a corresponding cumulative quantity, the number of pairs in the data (in MC sets) separated by the angular distance less than a given one. The significance of the excess (if any) at a given scale δ is then characterized by the p-value $P(\delta)$ defined as the fraction of MC sets that have the number of pairs separated by angles less than δ larger or equal than that in the data. This p-value is presented in Fig. 8 for the TA data sets with three energy thresholds. Low values of $P(\delta)$ indicate incompatibility with isotropy at the angular scale δ. As one can see from the plot, the two low-energy subsets are compatible with isotropy, while the high-energy one shows some deviations from isotropy at angular scales $20^\circ - 40^\circ$.

6.3 Hot Spot

Based on the 5-yr data event set with $E > 57$ EeV, the TA has reported a concentration of events ("hot spot") in the direction $(146^\circ.43^\circ)$ in equatorial coordinates of the radius $\sim 20^\circ$ with the post-trial significance of 3.4σ [7]. Here we present an update of this result with the 7-yr data set.

A special data set was compiled for the analysis of Ref. [7] which has even looser cuts than in the anisotropy data set, resulting in even larger statistics. The 5-yr set contains 72 events with $E > 57$ EeV, while the 7-yr set contains 109 events (37 were detected in 6th and 7th year of operation). The sky map of the 7-yr events in equatorial coordinates is shown in Fig. 9, left panel. Of the events detected in the 6th and 7th year, 4 more were found within the hot spot region.

The significance of the excess in the spot region was estimated in the 7-yr set in the same

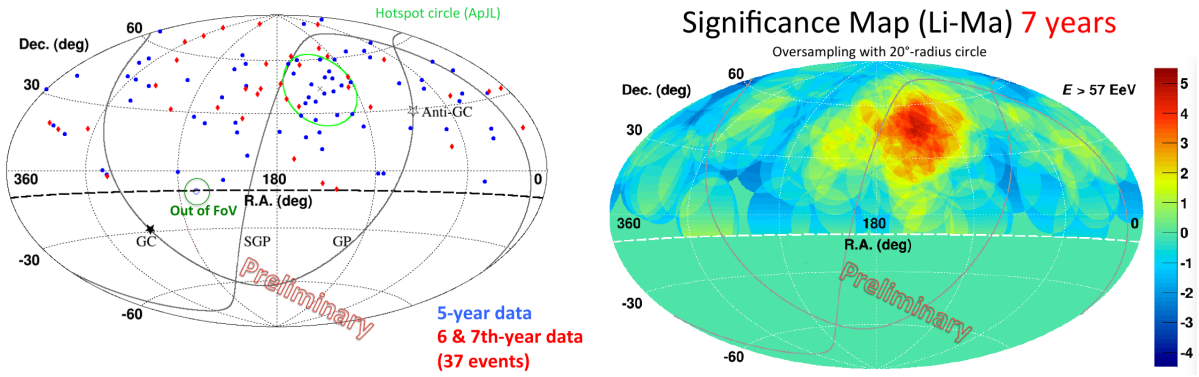

Figure 9 – *Left panel:* The sky map of 7-year TA events. 5-year data (blue points) and the 6th and 7th year (red points) are shown separately. The cross and the green circle represent the position and radius of the 5-yr hot spot. *Right panel:* The significance of local excesses/deficits in the TA 7-yr data set with $E > 57$ EeV when over-sampling with the 20° radius circular window.

way as described in Ref. [7]. The TA field of view was over-sampled with a moving circle of a given radius (15°, 20°, 25°, 30° and 35° radii were tried). For each position and radius of the circle, the significance of the excess/deficit in that circle was calculated by the Li-Ma method in the same way as in Ref.[7]. The resulting significance map is shown in Fig. 9, right panel. The maximum excess has the significance of 5.07σ and corresponds to 24 events observed within the circle while 6.88 were expected for the isotropic UHECR distribution.

To calculate the global significance a large number of Monte-Carlo sets with the same number of events were generated assuming isotropic UHECR distribution. For each set the same search of maximum excess was performed as in the real data. The fraction of MC sets where the excess of the same or larger significance as in the data was found gives the post-trial significance. This was found to be 3.4σ, the same as in the 5-yr data.

A blind search in the 6th and 7th data separately with the parameters of the circle fixed to the values determined in Ref.[7] reveals 4 events in the hot spot region while 2.31 are expected from an isotropic background. The probability of this excess in $P = 0.2$.

6.4 Correlation with LSS

Given the excess of events in a particular region of the sky in the highest energy data set, the question arises whether this region corresponds to any known astrophysical structure. Assuming the UHECR sources are sufficiently numerous, their distribution in space must trace the distribution of matter. Because of the relatively small propagation horizon at the highest energies, one may expect larger UHECR flux from the directions of nearby ($50 - 100$ Mpc) mater concentrations. The matter distribution in the nearby Universe is known from complete galaxy catalogs, e.g., the 2MASS catalog [8] and its derivatives. Treating each galaxy as an UHECR source and taking into account propagation effects and catalog selection biases as described in Ref.[5], one can calculate the expected UHECR flux. Assuming a pure proton composition, the expected flux depends on a single parameter, the smearing angle θ. An example of such calculation at $\theta = 6°$, with the flux modulated by the TA exposure, is shown in Fig. 10, left panel, in equatorial coordinates. The higher flux values are represented by darker gray. Letters mark nearby structures: UM – Ursa Major cluster, Co – Coma cluster, V – Virgo cluster, PP – Perseus-Pisces cluster. The white dots correspond to TA events with $E > 57$ EeV. The hot spot center is marked by the yellow cross.

Whether the TA events follow isotropy or the model expectation at a given vale of θ can be checked by an appropriate statistical test. In the TA analysis, the "flux sampling" test is used[9]. For each value of θ the compatibility with the isotropy or with the expectation from the local structures can be tested. The resulting p-values are presented in Fig. 10, right panel, as a

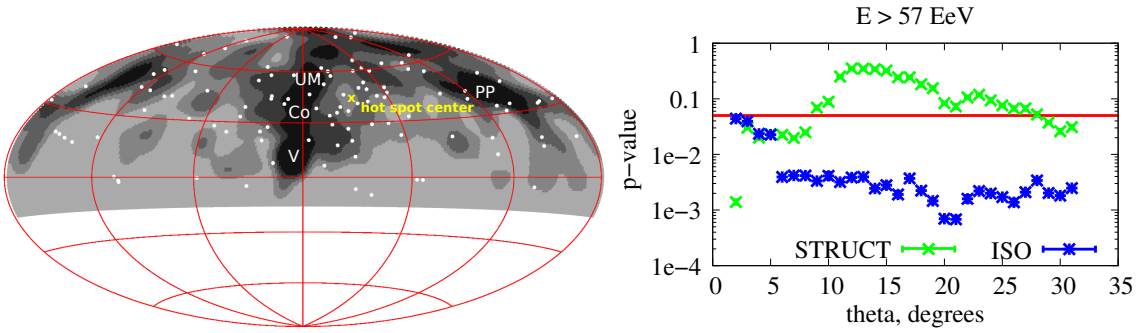

Figure 10 – *Left panel:* sky map of the flux expected in the model where sources follow the matter distribution. Darker regions correspond to higher flux. While dots are TA events with $E > 57$ EeV. *Right panel:* P-values of a statistical test for compatibility with isotropy (blue) and the model where sources are tracing matter, as a function of the smearing angle θ (green). Red line marks the 95% confidence level.

function of the angle θ. Isotropy is disfavored, while the data are compatible with the structure model at most (except the smallest) values of θ.

6.5 Other searches

The discrepancy between the TA and Auger spectra at highest energies may be related to the presence of the hot spot in the TA data or, more generally, to the dependence of the spectrum on the direction such that the Northern and Southern hemisphere spectra are different. This difference could arise from the inhomogeneous source distribution combined with the propagation effects: at high energies more particles will reach the Earth from the directions where sources are closer, if not significantly deflected. The regions of spectral differences may be searched for in a way similar to the analysis in sect. 6.3. Concretely, one defines a circle of given radius and

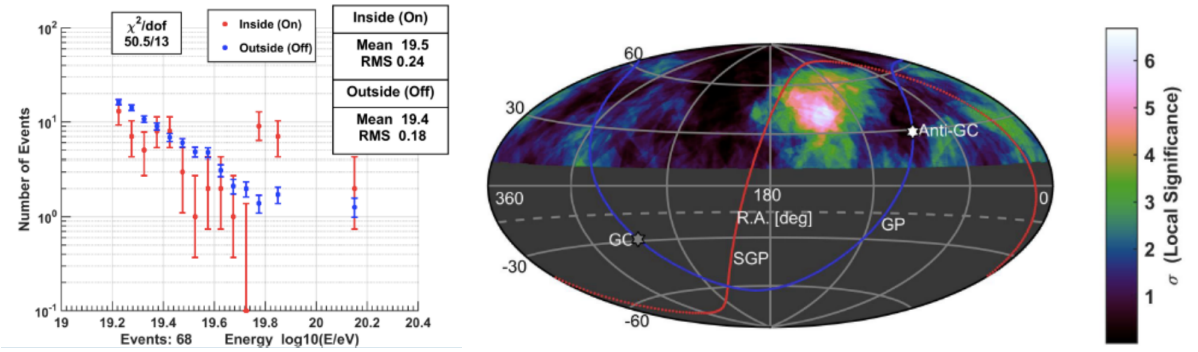

Figure 11 – *Left panel:* The energy spectra in the hot spot region (red) and outside (blue). *Right panel:* Sky map of local significance of spectral differences between the inside and outside of a moving circular window.

position to be an "on-source" region, while the rest of the sky an "off-source" region. The on- and off-source spectra can be compared by the binned χ^2-test. An example of such a comparison, with the on-source region being a circle of 20° around the hot spot is shown in Fig. 11, left panel. The on-source (red) and off-source (blue) spectra are clearly different.

The way to determine the statistical significance of this difference that takes into account that the presence of the hot spot in the highest-energy set was known in advance, is to test other circle positions and radii, and then take a statistical penalty for multiple trials. When this procedure is applied to the TA data it results in the map of local significance of the on- and off-source spectral differences; this map is shown in Fig. 11, right panel. The maximum local significance 6.7σ is indeed reached at the circle position close to the hot spot center. The global significance (after accounting for trials) can be calculated by repeating exactly the same search procedure for many simulated sets and determining the fraction of sets in which the maximum

significance was equal or higher than 6.7σ. Such calculation shows that the global significance of the spectral differences in the on-spot and off-spot regions is 4.0σ.

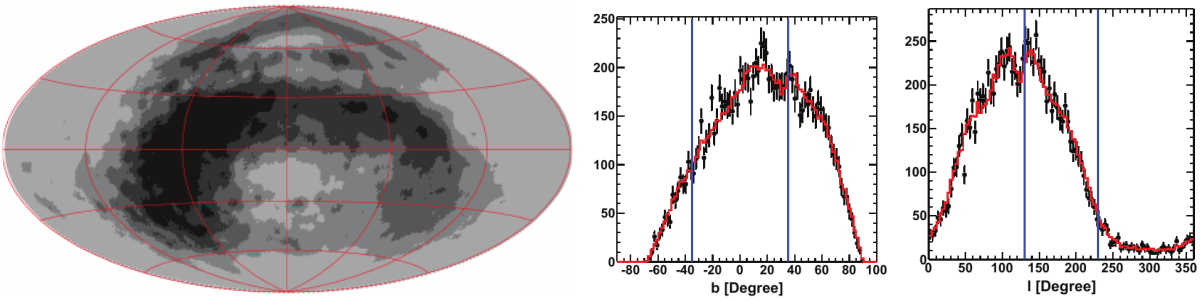

Figure 12 – *Left panel:* The sky map of the flux of 1 EeV protons expected form Galactic sources. *Middle and right panels:* the distribution of the TA events with energies between 10^{18} eV and $10^{18.5}$ eV in the galactic latitude and longitude (black dots) vs. the expectation for an isotropic incoming flux derived by the MC simulation (red line). Blue lines indicate the regions of largest expected deviations in case of contribution of Galactic protons.

We have discussed so far the highest energy end of the UHECR spectrum with $E > 10$ EeV, the reason being that the magnetic deflections decrease with energy. Interesting conclusions, however, can also be derived from a nearly isotropic distribution of UHECR at much lower energies around 10^{18} eV. This energy range is special in that protons change their propagation from a quasi-ballistic regime at higher energies to a diffusive one at lower energies. For protons of the Galactic origin, in the transition region one can have both the accumulation of the flux typical of a diffusive regime, and a strong anisotropy characteristic of the ballistic one [10]. As an example, in Fig. 12, left panel, we show the sky distribution of the flux of Galactic protons at 10^{18} eV. Strong anisotropy is evident. Comparing this expectation with the TA data one can constrain the fraction of protons of the Galactic origin at these energies to be less than $\sim 1\%$ [11]. Fig. 12, middle and right panels, shows the actual distributions of the TA events (black dots with error bars) in right ascension and declination as well as the expectation from the uniform distribution (red line) obtained from the MC simulations. Blue vertical lines indicate the bands where most of the deviation from isotropy is expected for the Galactic proton component. Perfect agreement of the data with the isotropic simulations leave little room for an admixture of such a component.

7 Conclusions

To summarize, by now the TA has been operating for 9 years. The data collected during the first 7 years of operation allowed us to measure the spectrum of UHECR over 4.5 orders of magnitude in energy starting from $\sim 10^{15.5}$ eV and up to $\sim 10^{20}$ eV, all with a single experiment. Several features were identified, in agreement with other experiments.

The uncertainty in the mass composition of UHECR remains a bottleneck limiting further progress (in particular, interpretation of the spectral features). Several analyses performed at TA and presented here indicate a light composition at energies above $10^{18.2}$ eV, consistent with pure protons, but also consistent with the light mix similar to the one preferred by the Auger results. Insufficient statistics and uncertainties in hadronic models are among the factors that limit the accuracy of the mass composition measurement.

The arrival directions of the UHECR observed by TA in the Northern hemisphere show a remarkable degree of isotropy at all except highest energies where the concentration of events — the hot spot — has been identified. The significance of this feature did not increase in the 7-yr data as compared to the 5-yr data set where it has been first found and remains at the level of 3.4σ (post-trial). Its interpretation is unclear at present. A significant increase in statistics at highest energies is required to either confirm or rule out the presence of this feature. This will

be achieved in a few years with the TA×4 detector which is now being constructed at the TA site.

Acknowledgments

The work of PT is supported by the IISN project 4.4502.16.

References

1. T. Abu-Zayyad *et al.* [Telescope Array Collaboration], Nucl. Instrum. Meth. A **689** (2013) 87 [arXiv:1201.4964 [astro-ph.IM]].
2. H. Tokuno *et al.*, Nucl. Instrum. Meth. A **676** (2012) 54 [arXiv:1201.0002 [astro-ph.IM]].
3. T. Abu-Zayyad *et al.* [Telescope Array Collaboration], Astropart. Phys. **48**, 16 (2013) [arXiv:1305.6079 [astro-ph.HE]].
4. V. Berezinsky, A. Z. Gazizov and S. I. Grigorieva, Phys. Rev. D **74** (2006) 043005 [hep-ph/0204357].
5. T. Abu-Zayyad *et al.* [Telescope Array Collaboration], Astrophys. J. **757**, 26 (2012) [arXiv:1205.5984 [astro-ph.HE]].
6. T. Abu-Zayyad *et al.* [Telescope Array Collaboration], Astrophys. J. **768** (2013) L1 [arXiv:1205.5067 [astro-ph.HE]].
7. R. U. Abbasi *et al.* [Telescope Array Collaboration], Astrophys. J. **790** (2014) L21 [arXiv:1404.5890 [astro-ph.HE]].
8. M. F. Skrutskie *et al.*, Astron. J. **131**, 1163 (2006)
9. H. B. J. Koers and P. Tinyakov, JCAP **0904**, 003 (2009) [arXiv:0812.0860 [astro-ph]].
10. P. G. Tinyakov, F. R. Urban, D. Ivanov, G. B. Thomson and A. H. Tirone, Mon. Not. Roy. Astron. Soc. **460**, no. 4, 3479 (2016) [arXiv:1511.01333 [astro-ph.HE]].
11. R. U. Abbasi *et al.*, Astropart. Phys. **86**, 21 (2017) [arXiv:1608.06306 [astro-ph.HE]].